Surface State Dissipation in Confined ^{3}He-A

Alexander J. Shook,* Emil Varga, and John P. Davis†
Physics Department, University of Alberta.
(Dated: October 6, 2023)

We have studied the power dependence of superfluid Helmholtz resonators in thin (750 and 1800 nm) rectangular channels. In the A-phase, we observe a non-linear response for velocities larger than a critical value. The small size of the channels stabilizes a static uniform texture, which eliminates dissipative processes produced by changes in the texture. For such a static texture, the lowest velocity dissipative process is due to the pumping of surface bound states into the bulk liquid. We show that the temperature dependence of the critical velocity observed in our devices is consistent with this surface state dissipation. Characterization of the force-velocity curves of our devices may provide a platform for studying the physics of exotic surface bound states in superfluid ^{3}He.

One of the defining features of superfluidity is the ability to flow without dissipation for velocities below a critical value [1]. The Landau criterion states that this velocity threshold is set by a local minimum in the dispersion relation of the lowest energy excitation of the system [1]. For fermionic superfluids, the relevant energy scale is the superfluid gap, Δ_p, which is the energy required to excite a quasiparticle from the Fermi surface, and the Landau critical velocity is therefore $v_L = \Delta_p/p_F$ [2].

Implicit in the arguments of Landau is the assumption that the gap is both spatially invariant and constant for all momentum states. In superfluid ^{3}He the latter assumption holds only for the bulk B-phase, which has an isotropic gap. Near a surface however, the gap becomes suppressed and develops separate parallel and perpendicular components [2]. The suppression of the gap near the wall also breaks the former assumption and allows for bound states with energies less than the bulk gap. Experiments studying oscillating macroscopic objects in ^{3}He-B have shown that there is a sub-Landau critical velocity threshold at which bound states are emitted from a moving surface, leading to an observable change in dissipation [3, 4]. Characterization of the coupling of these mechanical oscillators to fluid flow has proven to be a valuable tool for studying surface-bound states in ^{3}He-B [3–8]. These surface bound states are of interest not only from the perspective of understanding ^{3}He hydrodynamics [9] and quantum turbulence [10, 11], but also as a condensed matter realization of exotic quasiparticles such as Weyl or Majorana fermions [12–21].

The use of flow experiments to study bound states in the A-phase is limited due to the complexity that arises from the anisotropy of the A-phase gap. There exists an anisotropy axis $\hat{\ell}$, which points in the direction of a Cooper pair's orbital angular momentum, along which the superfluid gap closes at two point nodes (see Fig. 1c). Since the A-phase exhibits long-range spatial ordering in the orbital angular momentum of Cooper pairs, $\hat{\ell}(\vec{r})$ is a vector field, or texture, which may vary smoothly in space over distances larger than the coherence length. The orientation of this texture couples both to superfluid phase gradients (i.e., flow), and to spin degrees of freedom [2]. In the absence of other orientational effects, the tendency of the $\hat{\ell}$-texture is to align with the superfluid flow velocity $\vec{v}_s$ [22].

Naively this may seem to undermine the possibility of dissipationless flow in the A-phase since excitations can be produced for arbitrarily small velocities at the gap nodes, however for constant flow with a static texture this is not the case. A-phase superfluid flow can be stable even when aligned with $\hat{\ell}$ because only a small number of states exist near the nodes. These states quickly fill when the fluid begins to flow, but once filled do not contribute to dissipation [23]. This produces a non-linear relationship between the superfluid velocity and momentum density,

$$\vec{j}_s = \rho_s(v_s)\vec{v}_s, \tag{1}$$

because the superfluid density, ρ_s, decreases with increasing velocity as excitations are produced. The momentum

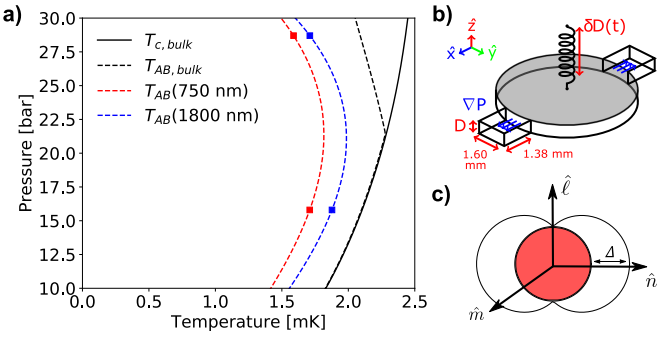

FIG. 1. A-phase flow. (a) Simplified phase diagram showing the range of temperatures where the A-phase exists for 750 and 1800 nm channels. Note that the A-phase is stabilized to lower temperatures and pressures by the tight confinement [42]. (b) Drawing of the confined Helmholtz resonator volume. (c) Momentum space plot of the Fermi surface (red) and the gap $\Delta_p = \Delta_A\sqrt{1-(\hat{p}\cdot\hat{\ell})^2}$ which goes to zero at the poles aligned with the anisotropy vector $\hat{\ell}$.

* ashook@ualberta.ca
† jdavis@ualberta.ca

density, $j_s(v_s)$, has a local maximum known as the maximum pair breaking current [2]. This relationship assumes the system is always near equilibrium such that the available states are all filled. There is, therefore, no special velocity at which dissipation onsets for this static texture, constant flow, case.

In cases where the texture is dynamic, the motion of $\hat{\ell}$ changes the gap, and therefore dissipates energy by creating new excitations as it moves [24]. Further complexity is added by the geometry of the superfluid container since the boundary conditions require the $\hat{\ell}$-texture to be perpendicular to surfaces. This means that ^{3}He-A flowing over a surface can produce a textural gradient where $\hat{\ell}$ is parallel to the flow far from the wall, and perpendicular at the surface [22]. The characteristic length-scale over which the texture rotates 90 degrees is the healing length, $\xi^A_{\rm heal} \sim 8$ μm [2]. For bulk systems, where all dimensions are large compared to the healing length, the texture can become a hydrodynamic variable that exhibits complicated behavior [25–30]. Systems, where one or more dimensions are small compared to the textural healing length tend to lock a particular texture in place. This can be seen in the literature by comparing a number of experiments with varying degrees of confinement [31–39].

A notable investigation of A-phase dissipation was carried out by Bagley et al. using a torsional pendulum, housing helium channels 49 μm in height [32]. When a relaxation time associated with the orbital texture was longer than the oscillation period the texture was essentially static, but when the two timescales were comparable a viscosity associated with the dynamic texture persisted at arbitrarily low velocities due to the motion of the texture. Parpia and Reppy studied oscillatory flow through an 18 μm diameter orifice, which showed constant dissipation until a single critical velocity (1.5 - 2.5 mm/s) [33].

Experiments with a higher degree of confinement have been achieved by using fine filters with average pore sizes of 8 μm [35], and 0.8 μm [39, 40]. In the case of Manninen et al. an additional dissipation regime was observed depending on if the temperature was above or below the bulk T_{AB} line. An interpretation of this result was offered based on a calculation for a cylindrical channel connecting two A-phase bulk reservoirs, where a phase gradient may be unwound by rotating the $\hat{\ell}$-texture at the ends of the channel [41].

In order to study the role that surface states play in A-phase dissipation, it is therefore desirable to create a parallel plate geometry with confinement much smaller than the healing length [42–46], ensuring a uniform texture. To this end, we have used our nanofluidic devices called Helmholtz resonators that have been described in previous publications [42, 47–49]. The devices are comprised of bonded quartz chips that have been etched to create a small volume sandwiched between the chips. The shape of this space is a circular basin (3.5 mm radius), with two 1.60×1.38 mm rectangular channels connecting it to the external helium bath (see Fig. 1b). The thickness of the enclosed space is constant throughout. The two devices used in this experiment had thicknesses of $D = 750 \pm 12$ and 1800 ± 12 nm.

Aluminum electrodes are patterned onto the quartz creating a parallel plate capacitor inside the basin. The volume of the basin can be slightly decreased by an electrostatic force between the capacitor plates. When this plate motion is driven resonantly with the Helmholtz mode of the channels, fourth sound is driven. The normal fluid does not move in the channels because the viscous penetration depth, δ, is large compared to the confinement ($\delta \approx 1$ mm $\gg D$) [50]. Furthermore, the confinement is also small compared to the healing length ($D \ll \xi^A_{\rm heal} \approx 8\,\mu$m) [2]. We therefore expect the texture to be uniformly aligned in the highly confined direction, $\hat{z}$. The fluid very close to the side walls may be an exception, but this represents a small fraction of the total volume and therefore is expected to have a negligible impact on the average mass current.

The capacitance of the Helmholtz resonator fluctuates in time when driven. We make use of a balanced General Radio 1615-a capacitance bridge that outputs a current proportional to the derivative of the time-varying capacitance. This current is fed into an SR570 trans-impedance amplifier that converts the current into a voltage signal, then is demodulated by a Zurich HF2LI lock-in amplifier. The measured capacitance signal responds to changes in the basin fluid mass when the fourth sound resonance is driven. A model of this system, described in the supplementary material [51], relates the spatially averaged mass current, $\langle j_s \rangle$, to the measured detector voltage via the equation

$$\langle j_s \rangle = \frac{(1+2\Sigma)}{2C_0 R_{\rm trans}} \left(\frac{\rho A D}{a} \right) \frac{V_{\rm DET}}{V_{\rm DC}}. \qquad (2)$$

Here, C_0 is the undriven capacitance, $R_{\rm trans}$ is the current to voltage conversion factor of the transimpedance amplifier, ρ is the total mass density of the ^{3}He, V_{DC} is a bias voltage used to enhance the signal, A is the area of the basin, a is the cross-sectional area of the channel, and Σ is a small correction factor to account for the finite compressibility of the helium.

By performing repeated power sweep measurements of the Helmholtz resonance, we are able to measure the drive dependence of the resonance amplitude [47]. As shown in Fig. 2, for low drives there is a linear regime, where the peak amplitude is proportional to the drive voltage, suggesting that the superfluid density is independent of drive. Once the peak of the resonances crosses a critical value, V_c, there is a secondary regime where the amplitude increases at a slower rate and the line shape begins to flatten at the top of the resonance. The amplitude saturates for large drive voltages, suggesting that there is a maximum momentum density that we cannot drive the resonator beyond.

We characterize this effect by recording the detector voltage at which the slope changes for both devices at

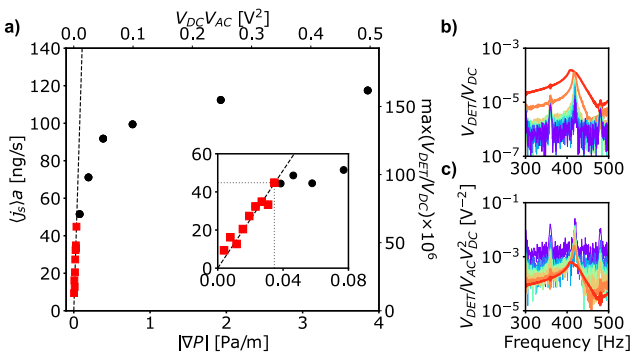

FIG. 2. Characterizing the non-linear regime. (a) The maximum detector voltage max($V_{\rm DET}$) for the 750 nm device at 22.45 bar and 2.08 mK is plotted as a function of the drive voltage $V_{\rm AC}$. The bias voltage $V_{\rm DC}$ is held constant throughout the experiment. On the opposite axes, the detector voltage has been converted into a mass current $\langle j_s\rangle a \propto V_{\rm DET}/V_{\rm DC}$ and the drive has been converted into a pressure gradient $|\nabla P| \propto V_{\rm DC}V_{\rm AC}$. The inset highlights the linear drive regime and a critical value at which the slope abruptly changes. (b) Log plot of the Helmholtz resonance with drive voltages ranging from 0.1 to 100 mV. (c) The same resonances as in Fig 2b are shown but are normalized by a quantity proportional to the driving force. Near resonance the line shape distorts above the critical drive.

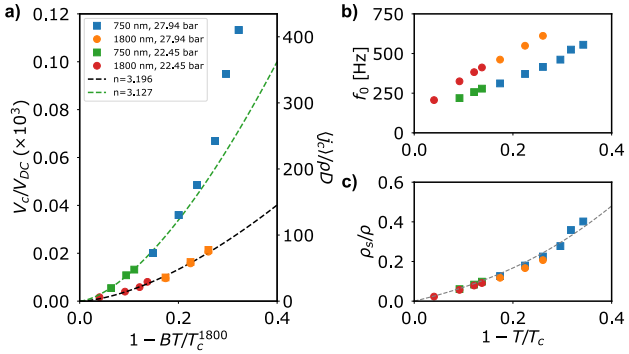

FIG. 3. Temperature scaling. (a) Plot of the peak voltage as a function of temperature for both devices at 22.45 and 27.94 bar. The dashed lines show fits to functions of the form $(1 - BT/T_c^{1800})^{n/2}$. The parameter B is used to rescale the critical temperature for the 750 nm device. The 22.45 bar and 27.94 bar data sets are fit together for the 1800 nm device but separately for the 750 nm device. (b) Measured frequency dependence of the Helmholtz modes. (c) Superfluid density of each device as calculated from the resonant frequency. The grey curve is the bulk superfluid fraction.

pressures of 22.45 and 27.94 bar, over a range of temperatures. This voltage threshold was then converted into a critical current using equation 2. These results are compiled in Fig. 3. The temperature was determined using the known temperature dependence of the superfluid density [2], referenced to a primary melting curve thermometer [52]. The temperature of each data point was computed using the resonant frequency of the fourth sound mode of the 1800 nm device. The fourth sound mode frequency changes according to the equation

$$\left(\frac{\omega_0(T)}{\omega_0(0)}\right)^2 = \frac{\rho_s}{\rho}, \tag{3}$$

where $\omega_0(0)$ is a function of the resonator dimensions, total fluid density, and the isothermal compressibility. Inversion of this curve allows the measured frequency to be converted into a temperature as described in the Supplementary Material [48, 51].

The temperature scaling was investigated by fitting 750 nm and 1800 nm amplitude data sets to a function of the form

$$\langle j_c\rangle = j_0(1 - BT/T_c^{1800})^{n/2}. \tag{4}$$

The prefactor B is included to account for the suppression of the critical temperature due to confinement. For the 1800 nm device $B = 1$, and for the 750 nm device it is the ratio of the two critical temperatures $B = T_c^{1800}/T_c^{750} = 1.042$. The value of this ratio is inferred by measuring the mode frequency as a function of temperature and extrapolating to zero frequency.

For the 1800 nm device, both pressure data sets are well fit by $n = 3.20$. For the 750 nm device, a similar curve, $n = 3.13$, can be fit to the data, but it deviates from this trend at lower temperatures. The fact that the A-phase persists to lower temperatures under higher confinement allows us to measure a wider range of temperatures in the 750 nm device. The deviation from a 3/2 power law appears to be a consequence of the fact that the superfluid fraction is approximately linear near T_c, but not at lower temperatures.

In light of the end effects observed by Manninen et al. [39, 40], it is also worth considering phase transitions of the bulk fluid outside the Helmholtz resonator. At 22.45 bar the bulk A to B transition occurs at $T_{AB} = 0.979T_c$ and for 27.94 bar it is $T_{AB} = 0.876T_c$. This means for the accessible range of temperatures the fluid outside the Helmholtz resonator was always B-phase.

The critical currents are converted into critical velocities, by taking the ratio $v_c = \langle j_c\rangle/\rho_s(v_c)$. Here $\rho_s(v_c)$ is the velocity-dependent superfluid density computed from the measured Helmholtz frequency at the critical value. We find the critical velocity curves for the two devices come close to falling onto one another (see Fig. 4) and are not inconsistent with a function of the form

$$v_c = v_0(1 - BT/T_c^{1800})^{1/2}, \tag{5}$$

which is similar to the temperature scaling of the conventional gaped Landau critical velocity. The temperature-independent prefactor of the fit is $v_0 = 2.67 \pm 0.09$ mm/s. The magnitude of the measured velocity is sufficiently small that textural explanations for the dissipation can be safely ruled out. Following Kopu and Thunburg [53] we take the velocity at which a textural transition should

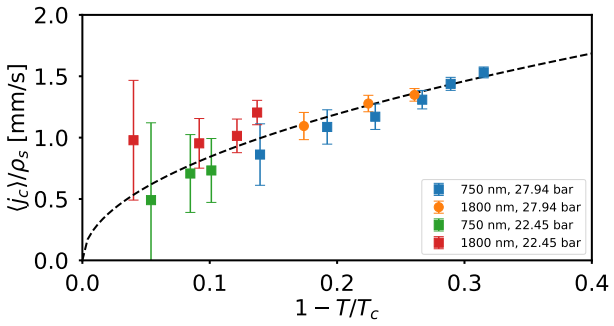

FIG. 4. Critical velocity. The critical current of the Helmholtz resonator is computed from the resonance amplitude at which the linear regime ends, and the superfluid density from the center frequency of the resonance. The ratio of these values is the critical velocity.

take place to be $\sqrt{3/4}\pi\hbar/2mD$, which is 38.20 mm/s and 15.91 mm/s for the 750 nm and 1800 nm channels respectively; significantly higher than the observed range of velocities.

Comparing our results to the DC flow experiments performed by Manninen et al. [39, 40], multiple dissipation regimes were observed only in cases where the end effects produced orbital viscosity. In experiments where the A-phase texture was static, there was no special velocity at which dissipation onsets, as expected for DC flow. This suggests that the dissipation onset velocity we observe is related to the dynamics of oscillatory flow resulting from our AC Helmholtz resonance.

To explain why oscillatory flow should generate dissipation above a critical velocity, we consider mechanical oscillator experiments performed in ^{3}He-B [3, 4]. Near the surface of a moving object, the gap is suppressed allowing for bound state excitations localized near the surface. Similar to the states near the A-phase nodes, these states do not contribute to dissipation once filled. When the mechanical oscillator velocity exceeds $v_L/(1+\alpha)$ and the oscillation period is large compared to the quasiparticle lifetime, surface excitations can escape into the bulk liquid [55]. Here α is a geometry-dependent constant related to backflow around a generic object, which is $\alpha = 2$ for a vibrating cylinder [55]. This allows for dissipation as the surface states are continuously populated and released.

The A-phase should also exhibit gap suppression within a few coherence lengths of the walls for diffuse scattering conditions [56], which we believe to be applicable to our devices due to surface roughness [42]. For the diffusive case, there does not seem to be any reason why the same velocity reversal process for scattering surface excitations into the bulk should not also occur in the A-phase. The primary difference is that the gap suppression near the anisotropy axis means that there are additional low-energy bulk states that can be populated. As with the DC flow case, we expect these to quickly become populated up to a level set by the maximum velocity. The threshold where dissipation onsets should correspond to the velocity at which the highest energy-bound state exceeds the lowest unfilled bulk energy state.

At finite temperatures, it is also necessary to consider thermal excitations. In the experiments of Castelijns et al. [3], and Bradley et al. [4], the temperatures were well within the ballistic regime ($T < T_c/8$ and $T \approx 140 - 190$ μK respectively) and the model used in their analysis assumes $T = 0$. Since the A-phase is stable at higher temperatures, our experiment is always in the hydrodynamic regime where thermal excitation can be expected to play an important role. Although existing models have focused on the $T = 0$ limit for simplicity, the fact that the critical velocity is proportional to the Landau velocity appears to be quite generic, since the argument depends only on the relative energy of the surface states compared to the bulk, not the processes by which the surface states are scattered. As pointed out by Castelijns et al. [3], it is possible at finite temperatures that quasiparticles play an intermediate role in allowing the bound states to escape into the bulk. The fact that the critical velocity we measure is proportional to $v_L \propto \Delta_A \propto \sqrt{1 - T/T_c}$ is therefore consistent with the dissipation due to surface states. A complete theoretical analysis of the A-phase in this temperature regime is desirable to predict the magnitude of the critical velocity.

In conclusion, we have carried out measurements of the force-velocity curves for oscillatory flow in ^{3}He-A in channels with thicknesses of 1800 and 750 nm. We find a dissipation onset at a critical velocity that has the same temperature scaling as the Landau critical velocity. This critical velocity is best explained by the pumping of surface bound states in our devices, an effect that has not previously been shown in ^{3}He-A. Our experiment studies channel sizes that are still large compared to the gap suppressed region where bound states are localized. In this regime, our measurement of the critical velocity does not show any notable dependence on the channel height or pressure. When the channel size becomes comparable to the coherence length, the gap suppression will extend across the entire channel [57] resulting in a reduced critical velocity. New generations of Helmholtz resonators have been developed to confine helium in channels as small as $D = 25$ nm [58]. Theoretical work suggests that the A-phase is favored over the planar phase even in this highly confined limit when strong coupling is considered [43, 45]. Using the pressure and temperature dependence of the coherence length, $\xi(P, T)$, gives us an in situ knob to change the ratio D/ξ. Studying the Helmholtz mode force-velocity curves as a function of this ratio is thus a platform for probing the properties of bound states in both ^{3}He-A and ^{3}He-B, which are predicted to be exotic Weyl [14, 17, 18, 21] and Majorana quasiparticles [59, 60].

ACKNOWLEDGMENTS

The authors acknowledge that the land on which this work was performed is in Treaty Six Territory, the traditional territories of many First Nations, Métis, and Inuit in Alberta. They acknowledge fruitful discussions with I. Boettcher and J. Maciejko, as well as support from the University of Alberta and the Natural Sciences and Engineering Research Council, Canada (Grant Nos. RGPIN-2022-03078, and CREATE-495446-17).

[1] I. M. Khalatnikov, *An introduction to the theory of superfluidity* (CRC Press, 2018).

[2] D. Vollhardt and P. Wolfle, *The superfluid phases of helium-3* (Courier Corporation, 2013).

[3] C. A. M. Castelijns, K. F. Coates, A. M. Guénault, S. G. Mussett, and G. R. Pickett, Landau critical velocity for a macroscopic object moving in superfluid ^{3}He-B: Evidence for gap suppression at a moving surface, Physical review letters **56**, 69 (1986).

[4] D. I. Bradley, S. N. Fisher, A. M. Guénault, R. P. Haley, C. Lawson, G. R. Pickett, R. Schanen, M. Skyba, V. Tsepelin, and D. Zmeev, Breaking the superfluid speed limit in a fermionic condensate, Nature Physics **12**, 1017 (2016).

[5] M. Skyba and P. Skyba, High quality tuning forks in superfluid ^{3}He-B below 200 μK, J Low Temp Phys **162**, 669 (2011).

[6] P. Zheng, W. G. Jiang, C. S. Barquist, Y. Lee, and H. B. Chan, Critical velocity in the presence of surface bound states in superfluid ^{3}He-B, Physical Review Letters **118**, 065301 (2017).

[7] M. T. Noble, S. L. Ahlstrom, D. I. Bradley, E. A. Guise, R. P. Haley, S. Kafanov, G. R. Pickett, M. Poole, R. Schanen, T. Wilcox, A.J. Woods, D.E. Zmeev, V. Tsepelin, *et al.*, Producing and imaging quantum turbulence via pair-breaking in superfluid ^{3}He-B, Physical Review B **105**, 174515 (2022).

[8] S. Autti, R. Haley, A. Jennings, G. Pickett, M. Poole, R. Schanen, A. Soldatov, V. Tsepelin, J. Vonka, V. Zavjalov, *et al.*, Quasiparticle transport in a two-dimensional boundary superfluid, arXiv preprint arXiv:2303.16518 (2023).

[9] J. A. Kuorelahti, S. M. Laine, and E. V. Thuneberg, Models for supercritical motion in a superfluid Fermi liquid, Physical Review B **98**, 144512 (2018).

[10] S. N. Fisher, M. J. Jackson, Y. A. Sergeev, and V. Tsepelin, Andreev reflection, a tool to investigate vortex dynamics and quantum turbulence in ^{3}He-B, Proceedings of the National Academy of Sciences **111**, 4659 (2014).

[11] V. Tsepelin, A. W. Baggaley, Y. A. Sergeev, C. F. Barenghi, S. N. Fisher, G. R. Pickett, M. J. Jackson, and N. Suramlishvili, Visualization of quantum turbulence in superfluid ^{3}He-B: Combined numerical and experimental study of Andreev reflection, Physical Review B **96**, 054510 (2017).

[12] S. B. Chung and S.-C. Zhang, Detecting the Majorana fermion surface state of ^{3}He-B through spin relaxation, Physical review letters **103**, 235301 (2009).

[13] Y. Tsutsumi, T. Mizushima, M. Ichioka, and K. Machida, Majorana edge modes of superfluid ^{3}He A-phase in a slab, Journal of the Physical Society of Japan **79**, 113601 (2010).

[14] M. A. Silaev and G. E. Volovik, Topological fermi arcs in superfluid ^{3}He, Physical Review B **86**, 214511 (2012).

[15] H. Ikegami, Y. Tsutsumi, and K. Kono, Chiral symmetry breaking in superfluid ^{3}He-A, Science **341**, 59 (2013).

[16] J. Maciejko, Y. Park, and S. B. Chung, Surface majorana fermions and bulk collective modes in superfluid ^{3}He-B, Bulletin of the American Physical Society **60** (2015).

[17] O. Shevtsov and J. A. Sauls, Electron bubbles and Weyl fermions in chiral superfluid ^{3}He-A, Physical Review B **94**, 064511 (2016).

[18] G. E. Volovik, On the chiral magnetic effect in Weyl superfluid ^{3}He-A, JETP letters **105**, 34 (2017).

[19] A. B. Vorontsov, Andreev bound states in superconducting films and confined superfluid ^{3}He, Philosophical Transactions of the Royal Society A: Mathematical, Physical and Engineering Sciences **376**, 20150144 (2018).

[20] H. S. Byun, J. Jeong, K. Kim, S. G. Kim, S. B. Shim, J. Suh, and H. Choi, Measuring angular momentum of $p_x + ip_y$ topological superfluids: A proposal, Physical Review B **98**, 024518 (2018).

[21] H. Wu and J. A. Sauls, Weyl fermions and broken symmetry phases of laterally confined ^{3}He films, Journal of Physics: Condensed Matter 10.1088/1361-648x/acf42b (2023).

[22] P. De Gennes and D. Rainer, Alignment of anisotropic superfluids by flow, Physics Letters A **46**, 429 (1974).

[23] G. E. Volovik, Superfluid properties of ^{3}He-A, Soviet Physics Uspekhi **27**, 363 (1984).

[24] M. Cross, Orbital dynamics of the anderson-Brinkman-morel phase of superfluid ^{3}He, Journal of Low Temperature Physics **26**, 165 (1977).

[25] G. Volovik and V. Mineev, Hydrodynamics of the a phase of superfluid ^{3}He, JETP Lett **24**, 561 (1976).

[26] N. Mermin and T.-L. Ho, Circulation and angular momentum in the a phase of superfluid helium-3, Physical Review Letters **36**, 594 (1976).

[27] P. Bhattacharyya, T. L. Ho, and N. D. Mermin, Stability of superflow in ^{3}He-A, Physical Review Letters **39**, 1290 (1977).

[28] M. Cross and M. Liu, Stability of the aligned state of ^{3}He-A in a superflow, Journal of Physics C: Solid State Physics **11**, 1795 (1978).

[29] A. L. Fetter, Hydrodynamic stability of ^{3}He-A, Physical Review Letters **40**, 1656 (1978).

[30] H. Kleinert, The two superflows in ^{3}He-A, Physics Letters A **71**, 66 (1979).

[31] R. Johnson, R. Kleinberg, R. Webb, and J. Wheatley, Heat flow in superfluid ^{3}He, Journal of Low Temperature Physics **18**, 501 (1975).

[32] M. Bagley, P. Main, J. Hook, D. Sandiford, and H. Hall, Direct observation of orbital dissipation and superflow collapse in ^{3}He-A, Journal of Physics C: Solid State Physics **11**, L729 (1978).

[33] J. M. Parpia and J. D. Reppy, Critical velocities in superfluid ^{3}He, Physical Review Letters **43**, 1332 (1979).

[34] A. J. Dahm, D. S. Betts, D. F. Brewer, J. Hutchins,

S. J. Saunders, and W. S. Truscott, Dissipation in the flow of ^{3}He-A and ^{3}He-B through a narrow rectangular channel, Physical Review Letters **45**, 1411 (1980).

[35] M. A. Paalanen and D. D. Osheroff, Dissipation of flow in superfluid ^{3}He-A, Physical Review Letters **45**, 362 (1980).

[36] V. Kotsubo, K. D. Hahn, and J. M. Parpia, Suppression of superfluidity of ^{3}He in cylindrical channels, Physical review letters **58**, 804 (1987).

[37] J. Kasai, Y. Okamoto, K. Nishioka, T. Takagi, and Y. Sasaki, Chiral domain structure in superfluid ^{3}He-A studied by magnetic resonance imaging, Physical Review Letters **120**, 205301 (2018).

[38] J. Daunt, R. Harris-Lowe, J. Harrison, A. Sachrajda, S. Steel, R. Turkington, and P. Zawadski, Critical temperature and critical current of thin-film superfluid ^{3}He, Journal of low temperature physics **70**, 547 (1988).

[39] M. T. Manninen, J. P. Pekola, R. G. Sharma, and M. S. Tagirov, Critical current of ^{3}He-A in narrow channels, Physical Review B **26**, 5233 (1982).

[40] M. Manninen and J. Pekola, Flow of superfluid ^{3}He through micrometer-size channels, Journal of Low Temperature Physics **52**, 497 (1983).

[41] E. Thuneberg and J. Kurkijärvi, Difficulties of supercurrents in narrow pores of ^{3}He-A, Physics Letters A **86**, 35 (1981).

[42] A. J. Shook, V. Vadakkumbatt, P. SenarathYapa, C. Doolin, R. Boyack, P.H. Kim, G. G. Popowich, F. Souris, H. Christani, J. Maciejko, and J. P. Davis, Stabilized pair density wave via nanoscale confinement of superfluid ^{3}He, Physical Review Letters **124**, 015301 (2020).

[43] P. S. Yapa, R. Boyack, and J. Maciejko, Triangular pair density wave in confined superfluid ^{3}He, Physical Review Letters **128**, 015301 (2022).

[44] N. Zhelev, T. S. Abhilash, E. Smith, R. Bennett, X. Rojas, L. Levitin, J. Saunders, and J. Parpia, The ab transition in superfluid helium-3 under confinement in a thin slab geometry, Nature communications **8**, 15963 (2017).

[45] C. Sun, A. Attar, and I. Boettcher, Superfluid phase transition of nanoscale-confined helium-3, arXiv preprint arXiv:2307.08808 (2023).

[46] L. V. Levitin, B. Yager, L. Sumner, B. Cowan, A. J. Casey, J. Saunders, N. Zhelev, R. G. Bennett, and J. M. Parpia, Evidence for a spatially modulated superfluid phase of ^{3}He under confinement, Physical Review Letters **122**, 085301 (2019).

[47] E. Varga, V. Vadakkumbatt, A. J. Shook, P. H. Kim, and J. P. Davis, Observation of bistable turbulence in quasi-two-dimensional superflow, Physical Review Letters **125**, 025301 (2020).

[48] X. Rojas and J. P. Davis, Superfluid nanomechanical resonator for quantum nanofluidics, Physical Review B **91**, 024503 (2015).

[49] E. Varga and J. P. Davis, Electromechanical feedback control of nanoscale superflow, New Journal of Physics **23**, 113041 (2021).

[50] J. Reppy, Superfluid density and viscosity measurements in liquid ^{3}He, Physica B+C **90**, 64 (1977).

[51] See Supplemental Material at `URL` for the derivation of this equation.

[52] D. S. Greywall and P. A. Busch, ^{3}He-melting-curve thermometry, Journal of Low Temperature Physics **46**, 451 (1982).

[53] J. Kopu and E. Thuneberg, Soliton-limited superflow in ^{3}He-A between parallel plates, Journal of Low Temperature Physics **124**, 147 (2001).

[54] A. Ahonen, J. Kokko, O. Lounasmaa, M. Paalanen, R. Richardson, W. Schoepe, and Y. Takano, Mobility of negative ions in superfluid ^{3}He, Physical Review Letters **37**, 511 (1976).

[55] C. Lambert, Theory of pair breaking by vibrating macroscopic objects in superfluid ^{3}He, Physica B: Condensed Matter **178**, 294 (1992).

[56] A. B. Vorontsov and J. A. Sauls, Thermodynamic properties of thin films of superfluid ^{3}He-A, Physical Review B **68**, 064508 (2003).

[57] L. J. Buchholtz, Superfluid ^{3}He-B in a realistic thin film: Gap function, Physica B: Condensed Matter **165**, 657 (1990).

[58] E. Varga, C. Undershute, and J. P. Davis, Surface-dominated finite-size effects in nanoconfined superfluid helium, Physical Review Letters **129**, 145301 (2022).

[59] Y. Tsutsumi and K. Machida, Edge current due to majorana fermions in superfluid ^{3}He-A and B-phases, Journal of the Physical Society of Japan **81**, 074607 (2012).

[60] H. Wu and J. A. Sauls, Majorana excitations, spin and mass currents on the surface of topological superfluid ^{3}He-B, Physical Review B **88**, 184506 (2013).